Toward Developing a Hydrodynamic Flow and Inundation Model of the Lower Pearl River

Paul McKay
and Cheryl Ann Blain
Naval Research Laboratory
Stennis Space Center, MS 39529-5004
Telephone: (228) 688–5664
Fax: (228) 688–4759

Abstract— **The lower Pearl River in Mississippi and Louisiana flows through extensive areas of intertidal marshes and floodplains and is subject to frequent floods due to upstream flows, local runoff and tidal and storm forcing. In order to improve flow and flood prediction capabilities, a hydrodynamic flow and inundation model for the lower Pearl River is being developed using ADCIRC by the river modeling group at the Naval Research Laboratory at Stennis Space Center. Image analysis techniques are applied to high resolution aerial photography of the Pearl River to extract the channel boundaries and a synthetic bathymetry is generated by fitting an idealized cross-section across the channel. A mesh is generated for the entire lower Pearl River from Bogalusa, LA to the coast.**

A separate mesh is created for a subregion of the East Pearl River and this model is validated against observations.

I. Introduction

The Pearl River drains approximately 8,600 sq.mi. (22,270 km^2) [1] in southeastern Louisiana and southwestern Mississippi in the Pine Meadows unit of the East Gulf Coastal Plain [2] (see Figure 1). Originating near Edinburgh, MS, the Pearl River flows south before splitting into two distinct channels west of Picayune, MS to form the East and West branches of the Pearl, which drain into Lake Borgne and the Mississippi Sound and eventually to the Gulf of Mexico. The East Pearl river serves as the political boundary between Louisiana and Mississippi. The West Pearl is the major stream of the pair with a mean flow approximately twenty times that of the East Pearl [3].

With, generally, 70% of the average annual rainfall of 68 inches (1.72 m) [4] occurring in the winter and early spring, flows are highest at these times, with generally low streamflows occurring in late summer and early fall. The area is frequently affected by tropical weather, including tropical depressions, storms and hurricanes, which can bring significant rain (greater than 30 inches (76 cm) [5]) as well as storm surge as high as 36 ft (11 m) [6]. With a tidal range of as much as 1 m on spring tide and 0.3 m on neap at the ocean mouth, flows in both the West, and especially the East, Pearl River show a strong tidal signal with tidal fluxes generally much greater than river outflow. Both channels regularly flood and drain the bordering intertidal marshes.

Flood events are quite common in both branches of the lower Pearl River and can be caused by high upstream discharge, local rainwater runoff, extreme high tides due to the coincidence of high spring tides with Ekman transport due to offshore forcing or surge tied to local storm events. Both channels of the lower Pearl are bordered by extensive floodplains which can be significantly inundated during high flood events. At their worst these flood events can cause significant physical and economic damage to communities on the river [7].

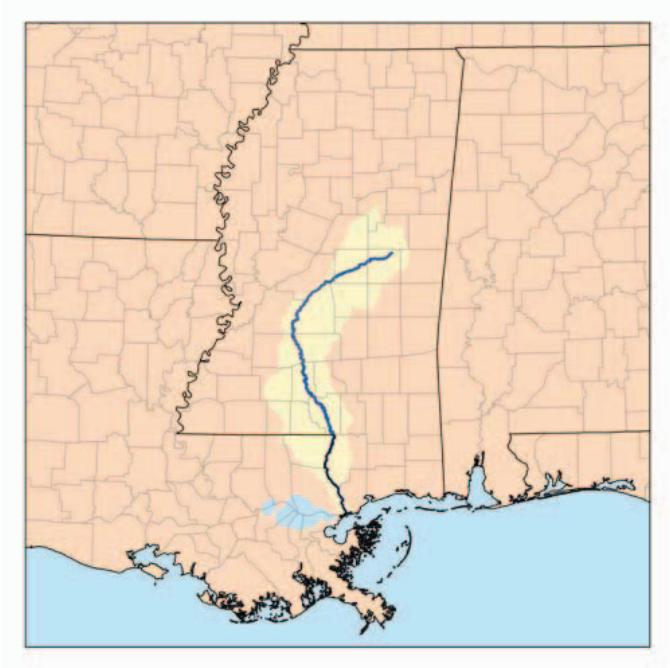

Fig. 1. The main channel of the Pearl River showing the drainage area (map courtesy of Karl Musser).

Currently, river stage and flooding predictions are issued by NOAA's Lower Mississippi River Forecast Center using a 1D hydraulic routing model which accounts for upstream flow, direct runoff and oceanic forcing. In order to aid in, and perhaps improve, these forecast capabilities, the river modeling group at the Naval Research Laboratory has begun to develop a two dimensional, depth-integrated, hydrodynamic model of the lower Pearl River and associated floodplains with the goal

0-933957-38-1/09/$20.00

of accurately modeling in-channel flows as well as flooding in response to upstream, oceanic and local forcing. This model is to be implemented using ADCIRC with an unstructured mesh derived from aerial photography of the Pearl River as well as measured topography and synthetic river bathymetry.

In this paper, Section II discusses work done in generating a mesh of the channel of the Pearl River, Section III discusses work done to validate a sub-region of this mesh and Section IV discusses the path forward and planned work.

II. Mesh Generation

The section of the lower Pearl River to be meshed runs from just below Bogalusa, LA to Lake Borgne and the Gulf of Mexico and is bounded by a box defined by 30°9'N to 30°42'N and 89°30'W to 89°50'W. In the absence of field measurements to establish the location of the river banks, the use of image analysis techniques applied to aerial, or satellite, photographs of a river to extract this information is becoming common [8] [9]. The area is fully covered by 1m resolution infrared Digital Orthoimagery Quarter Quadrangle (DOQQ) imagery which conforms to USGS standards. This imagery is housed at the LSU CADGIS laboratory and is freely available from the Louisiana Statewide GIS Atlas website (`http://atlas.lsu.edu/`) as MRSID compressed georeferenced TIFF imagery on the UTM 15 NAD 83 datum.

The main channel and major side channels of the Pearl River are covered by twenty five of these quarter quadrangle images, a typical one of which is shown in Figure 2. These images were decompressed and assembled into a georeferenced mosaic image using the open source openEV front end to the, also open source, Geospatial Data Abstraction Library (GDAL). This allowed them to be assembled into a seemless georeferenced tiff, 32,838 pixels by 76,674 pixels at 1 m per pixel, which occupied 7GB of disk space uncompressed. The image was then reduced to 4 m resolution, requiring 900 MB of space, so that it could be processed using a desktop workstation running 64 bit MATLAB.

A. Image Analysis

As the images were taken over a period of several days, with differing lighting and exposure, the mosaic was first equalized using a moving patch equalization filter which significantly reduced color and exposure differences across the image and which nearly eliminated lines between mosaic tiles.

The imagery is saved in 24 bit RGB (Red-Green-Blue) color space where each pixel is represented by a value for red, green and blue between 0 and 255. However since HSI (Hue-Saturation-Intenstity) color space more closely matches the way that human eyes perceive images [10], it is advantageous to convert the image into that colorspace. In HSI space the vaue of hue, ranging from 0 to 255, specifies the location of the pixel's color on a defined colorwheel (with blue in the range of 160), saturation specifies the amount of grey in the color, with 0 corresponding to pure grey and 255 to pure color, and intensity specifies lightness, or luminance, with 0 being black and 255 being bright light.

Fig. 2. A typical DOQQ image tile of the Pearl River (c3008934_nes_20.sid). Image center is at 30.4725° N, 89.7794° W

Ten subregions were isolated in the image, where the area of interest contained similar numbers of land and river pixels. Following a procedure similar to that used by Tanaka for the Nanakita River in Japan [11], histograms were generated for each channel of the image in each subregion. These histograms were then averaged across all of the areas for each channel of the image.

A clear separation between the hue values for land pixels and water pixels can be seen in Figure 3, with water pixels having a greenish-blue hue centered around a value of 135 and land pixels showing more spread but having a generally reddish-brown hue centered around a value of 60. Assuming a normal distribution for the hue value of water and selecting a criterion such that water pixels should have a hue value within two standard deviations of the peak water hue value, we can define an easily applied criteria for unsupervised classification of land and water pixels.

Applying this criteria to the region in Figure 2 selects all pixels which can be classified as water in this image. These results are then passed through a despeckling filter, which removes isolated small pixel groups while leaving the larger regions which are indicative of flowing water or large ponds. Figure 4 shows this overlain on the original image with water pixels indicated in red. As unsupervised classification is not capable of discriminating between the river channel and larger ponds, unconnected areas of water, such as the pond in the lower middle of Figure 4, must be manually removed. Further manual editing is required to connect water areas masked by

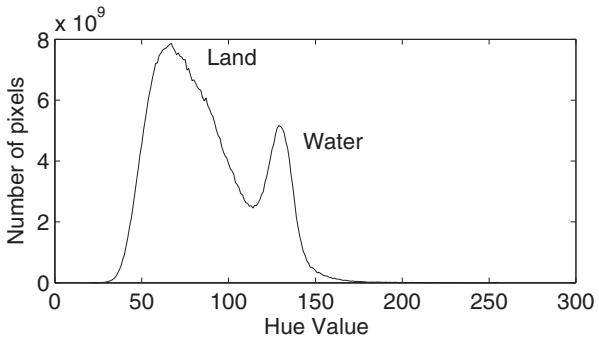

Fig. 3. Averaged histogram of hue values in the vicinity of the river channel.

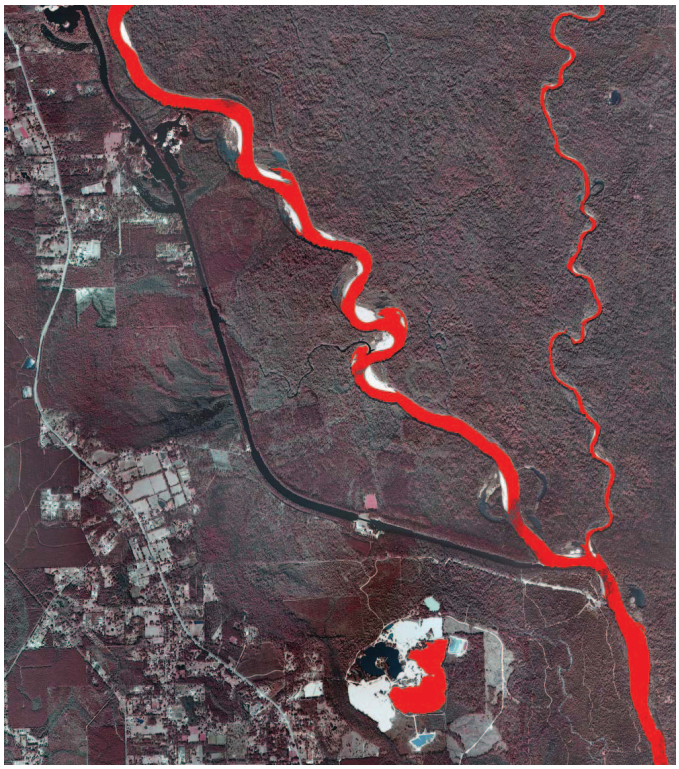

Fig. 4. Figure 2 with water pixels, as determined by applying the hue criterion, highlighted in red.

bridges, locks and trees or structures along the channel edge.

Once the image has been manually cleaned to remove these areas, the background is subtracted and a Laplace edge finding filter is used to find the single pixel width lines which bound the water area of interest. This is illustrated in Figure 5.

B. Mesh Generation

In order to generate the unstructured mesh we employ the NRL Mesh Create program [12] which requires an input of an ordered coastline as well as bathymetry which spans the entire domain. An ordered coastline can be extracted from the raster edge data, such as is seen in Figure 5, by employing an edge following algorithm to trace each edge and output it as a clockwise or counterclockwise ordered line.

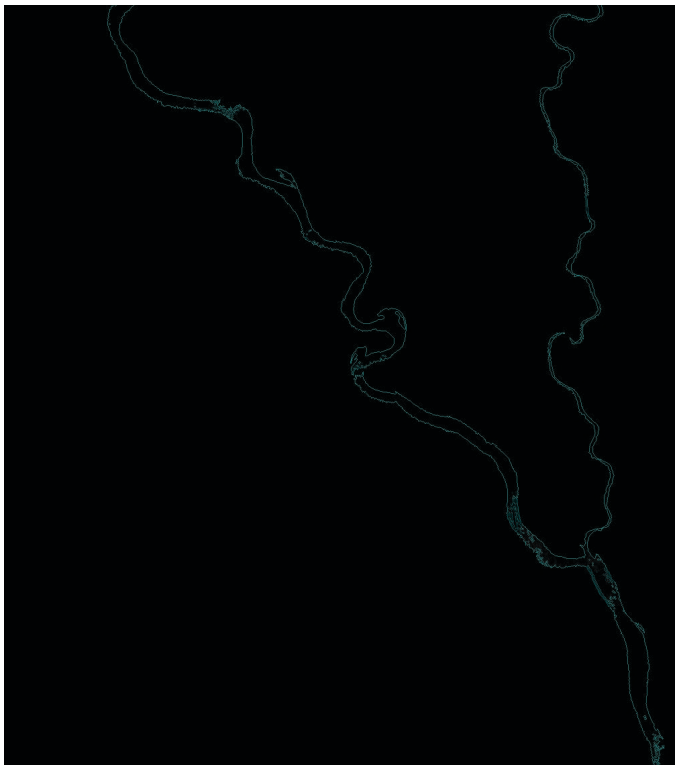

Fig. 5. Water edges as determined by a Laplace edge finding filter.

No measured bathymetry is available for the majority of the domain, except for a portion of the lower East Pearl River – as will be discussed later. Lacking any measured bathymetry, a synthetic bathymetry must be generated for the mesh. For each point identified as being a water point, approximately 4 million in the full river, a parabola [13] is fit spanning the channel along the shortest possible path and an initial depth is taken from that parabola. After the initial bathymetry is calculated, each point is averaged with its nearest neighbors to insure smooth transitions and avoid discontinuities, especially in areas where channels split or merge.

This ordered coastline and synthetic bathymetry are then used to generate an initial mesh. At the time of publication, this initial mesh is still undergoing mesh refinement and has yet to be run. It is estimated that the final mesh will have approximately 600,000 nodes and a mesh resolution which ranges from 4 m in the smallest channels and side creeks to 500 m at the ocean boundary.

III. Validation

As the full mesh is still being developed, as of the time of this writing, a separate sub-mesh was selected for validation of the model and method. This mesh covers the portion of the East Pearl River near and downstream of Stennis Space Center and is in a region for which detailed bathymetry is available along with some amount of validation data.

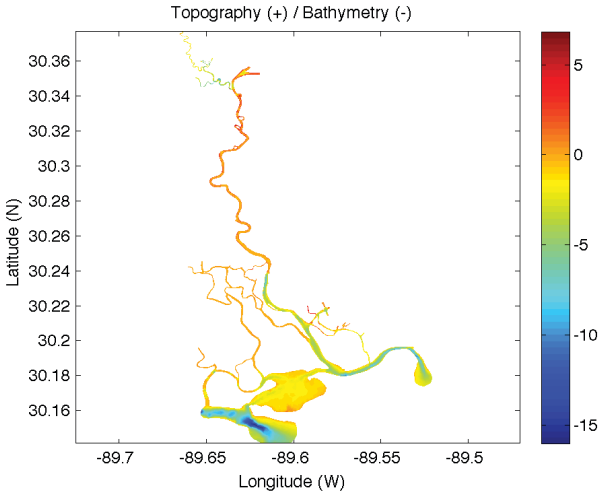

Fig. 6. Measured bathymetry in the East Pearl River subregion.

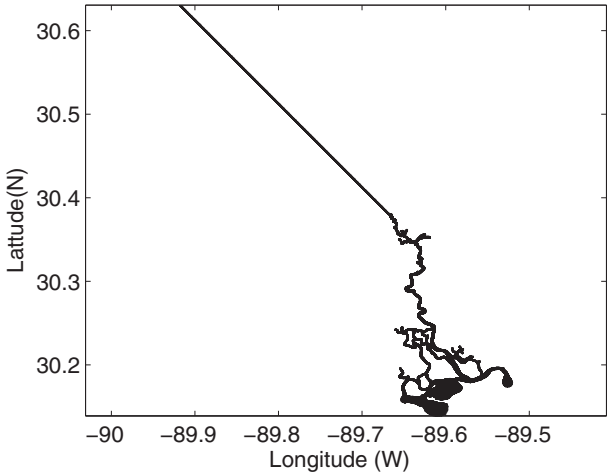

Fig. 7. East Pearl River submesh with upstream extension.

A. East Pearl River Sub-mesh

Detailed bathymetry is available, from a number of sources, for the lower portion of the East Pearl River from just upstream of Stennis Space Center to the ocean boundary (see Figure 6). Where bathymetric data sets overlap they have been averaged to create a single bathymetry file covering the whole of the lower East Pearl region. This has been combined with edge data from a mesh of the area previously created at NRL to generate a new mesh of the area of interest. This is an unstructured mesh with 80,452 nodes and 143,645 elements. Grid resolution varies from approximately 1 m in the smaller channels to 500 m in Lake Borgne and in the Mississippi Sound.

The upstream, or river flux, boundary is modeled using a defined flux (IBTYPE = 2) boundary condition which imposes a defined normal flow at the boundary nodes. As this has the effect of strongly damping the along channel tidal flows, which are not able to radiate through, and causes the flooding tidal waver to reflect and interfere with predicted elevations through the domain, it is necessary to artificially move this boundary far from the region of interest such that this damping effect becomes minimal in the true model domain [14]. For this reason the mesh was extended upstream as a virtual channel for a distance equal to 1.5 times the main channel length. This distance was found to be sufficient such that tidal flows are unimpeded through the river domain and the reflected tidal wave is dissipated before it interferes with elevations in the region of interest. The mesh, with this extension, is shown in Figure 7. River forcing is set to a constant value of 500 cfs. This corresponds to the mean measured flow near the upstream boundary of the mesh for the last two weeks of May 2009.

Tidal forcing is applied to the downstream open boundaries with six component harmonic tides (Q1, O1, K1, N2, M2, K2) taken from the Grenoble FES99 ADCIRC database. Many of the small side channels, particularly in the lower portion of the mesh, feed into small ponds and marshes. As such these have been left open as radiation boundary conditions allowing the tides to radiate through them. The period of interest, 18-31 May 2009, was selected as a period during which meteorological forcing was minimal and, as such, it has not been included in this test run.

B. Data Sources

Data to validate the model is available from a number of sources spanning the length of the main channel (see Figure 8). NRL maintains a long term flow mooring near the upper boundary of the mesh consisting of a side looking RDI HADCP which provides instantaneous cross-channel averaged velocities and estimated volume flux. The USGS maintains a streamflow monitoring station (number 301141089320300) at the CSX railroad bridge near Clairborne, MS which provides water depth and streamflow near the ocean boundary. During the months of May and June 2009 two additional moorings were placed along the axis of the East Pearl River (at the I-10 and Highway 90 bridges). These bottom mounted Aquatroll CTDs recorded water depth every 30 minutes throughout their deployment. There is, additionally, a USGS streamflow monitoring station located near the HADCP mooring which intermittently provides water depth and streamflow information.

C. Validation

The model was run in 2D depth-integrated barotropic mode for the period from 18 to 31 May 2009. River flux and tides were ramped up over a 21 day period prior to the period of interest. Velocity and depth were output for each node every hour. As the model run did not account for subtidal variations tied to forcing by wind and atmospheric pressure,

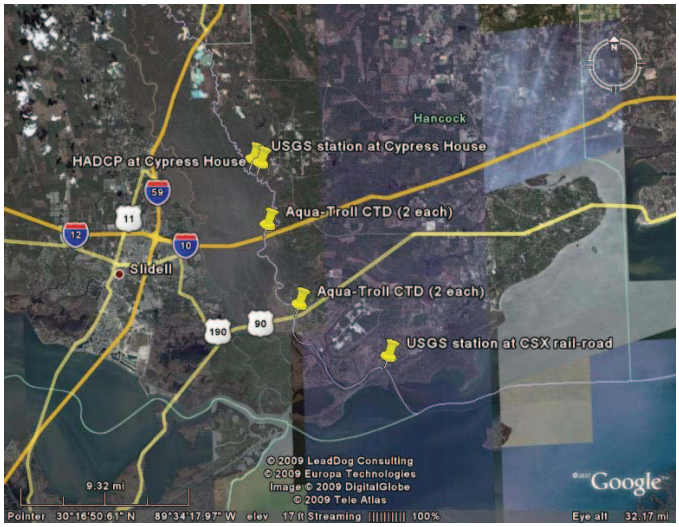

Fig. 8. Locations of East Pearl River moorings during May and June 2009. Figure courtesy of Wesley Goode.

all measured data was filtered, using a 3rd order 40 hour high pass Butterworth filter, to remove subtidal signals [15]. Once these subtidal signals were removed, the model and the data show very good agreement for both tidal variations in water depth and along channel velocity.

Figure 9 shows tidal variation in water depth, referenced to mean water level, at the CSX railroad bridge from 18-31 May 2009. The blue curve is the measured data and the red curve the model output. The model matches the phase of the measurements precisely while overpredicting the magnitude of the spring tide by approximately 3 % and matching it very well at neap tide.

Further upstream, at the I-10 Aquatroll mooring, we see similar results. Figure 10 shows the same data plotted for the I-10 mooring. As at the lower boundary, the model slightly overpredicts tidal height at spring tide, in this case by approximately 5 %. At neap tide the high tide is modeled precisely but the low tide is overpredicted, again by approximately 5 %. Both other mooring locations show similar results.

Comparing the measured cross channel average of the along channel velocity at the HADCP mooring to the model output (see Figure 11) the agreement is also good, however the model underpredicts maximum ebb (positive) velocities by as much as 15 % on spring tides. This is possibly due to inaccuracies in modeling river flux as constant in this case or perhaps to surface effects interfering with the cross channel HADCP velocity measurements.

Current maps produced for different regions of the Pearl River (see, for example, Figures 12 and 13, the locations of which are shown in Figure 14) show the expected flow patterns but there is, at present, no data available to validate these.

D. Validation of the Synthetic Bathymetry

In order to test the validity of the simple synthetic bathymetry which has been used in the main mesh, the real bathymetry of the validation model was replaced, node

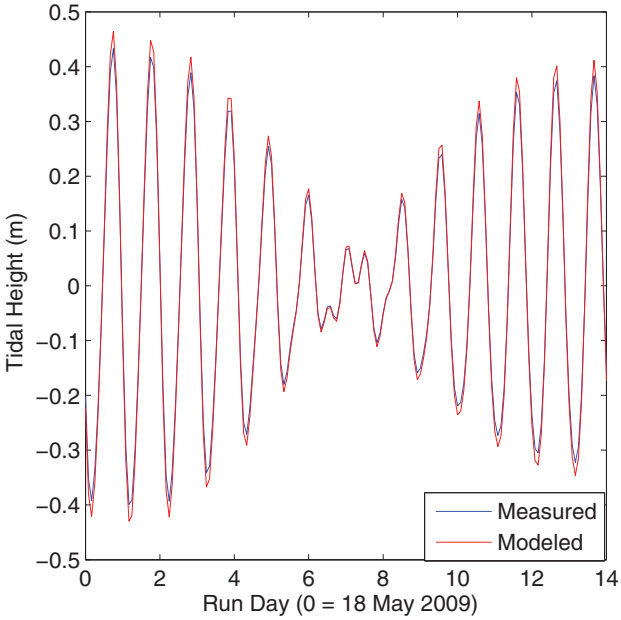

Fig. 9. Tidal variations in water depth at the CSX railroad bridge from 18 to 31 May 2009.

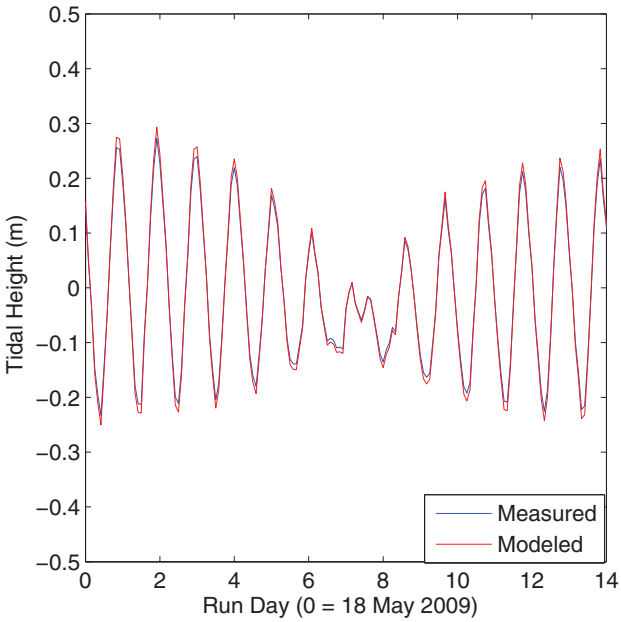

Fig. 10. Tidal variations in water depth at the I-10 mooring from 18 to 31 May 2009.

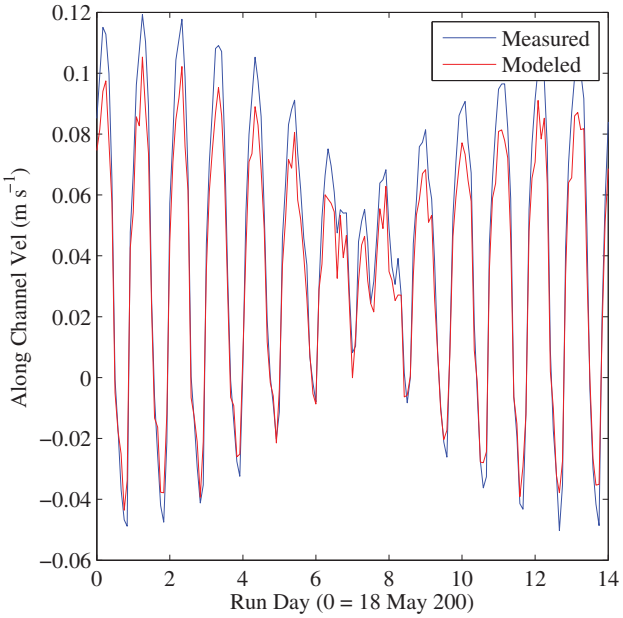

Fig. 11. Cross channel average of the along channel velocity at the HADCP mooring from 18 to 31 May 2009.

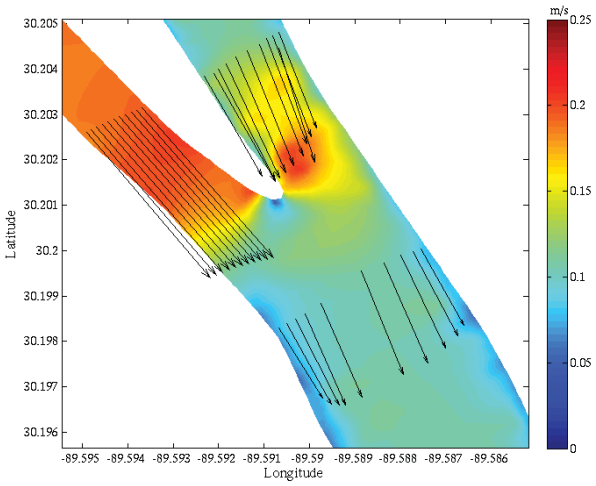

Fig. 13. Current map in the middle region of the East Pearl mesh at 1200 CST, 20 May 2009.

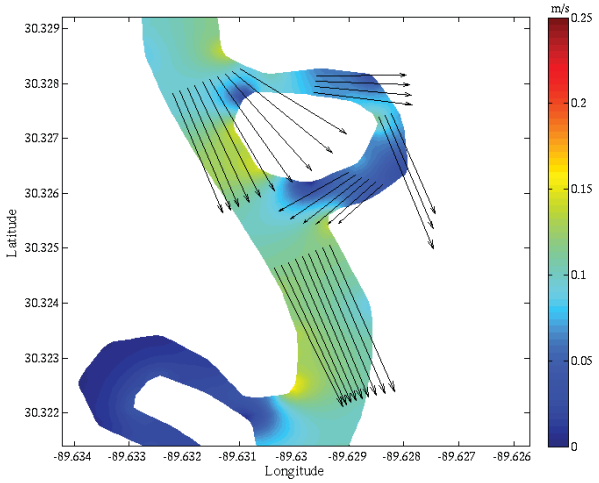

Fig. 12. Current map in the upper region of the East Pearl mesh at 1200 CST, 20 May 2009.

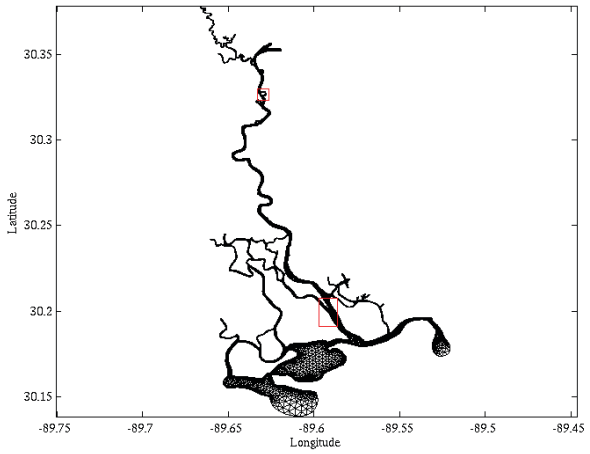

Fig. 14. Location of current maps in Figures 12 and 13.

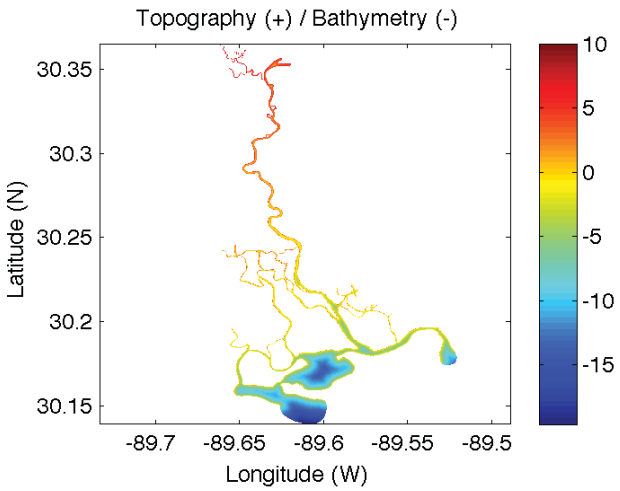

Fig. 15. Topographically adjusted synthetic bathymetry for the East Pearl River mesh.

by node, with a bathymetry based on a parabolic channel cross-section as described in Section II-B. As this synthetic bathymetry is referenced to mean sea level it does not account for the topographic slope of the area and thus does not allow for modeling of the gravity driven pressure gradient attributed to that slope. To correct for this, the synthetic bathymetry was merged with topographic data from the NGLI (Northern Gulf Littoral Initiative) three arc second topography of the region. The edges of the parabolic cross-sections were fixed to the topographic height from the NGLI data and the channel was modeled downwards from this new datum. This synthetic bathymetry is shown in Figure 15.

Comparing this synthetic bathymetry with the measured bathymetry shown in Figure 6, it appears that the synthetic bathymetry is a good approximation of main channel bathymetry, including the scour holes near channel junctions, but that it does not, and in fact can not, model either the shoaling regions in the channel or the channel meanders in which the thalweg is displaced to the left or right of channel center. The thalweg is constrained to be in the geometric center of the channel.

At the ocean boundary, the synthetic bathymetry does not model the deep scour channel created by the high tidal flows in the area and it significantly overestimates water depth, especially in Lake Borgne. As this bathymetry is based purely on horizontal geometry it can not model the sedimentation and scour processes which reduce or increase water depth in these areas. However since these are in regions of lesser interest in this modeling effort, and are near boundaries which are forced by tidal elevation referenced to mean sea level, there should be little effect on the overall solution.

It is apparent, especially near the upstream boundary, that the synthetic bathymetry overestimates the topographic height. This is likely due to the low resolution of the three arc second NGLI topography. However this error amounts to only 2.5 m over a length from the coast of 24.5 km and is not likely to be significant. For future work we are examining both USGS topography and LIDAR derived digital elevation models of the area as well.

Removing the topography from both sets of bathymetry, such that both are referenced to mean sea level at all cross-sections, and examining only the region of the main channel upstream of the obvious differences due to tidal and sediment processes, there is a maximum error in the main channel depth of 0.72 m where the synthetic bathymetry does not account for a shoal in the river. The RMS error for all points in the main channel is 0.21 m.

Near the ocean boundary and in Lake Borgne there is a maximum error of 10.13 m where the synthetic bathymetry greatly overpredicts depth in the shallow and sediment filled Lake Borgne.

IV. Future Work

Final refinement of the mesh, including both the East and West branches of the lower Pearl River, is expected to be complete shortly. The synthetic bathymetry generated for this mesh will be offset by the mean topography, as was described in Section III-D, and then merged with the available measured bathymetry for the lower section of the East Pearl River, shown in Figure 6..

This new model will then be validated against the measurements taken by the permanent moorings in the East Pearl River (described in Section III-B) and planned measurements of water depth to be taken in the heretofore ungauged West Pearl River.

Following this validation, the mesh will be extended to incorporate the floodplain around and between the two branches of the river using both USGS and NGLI topography. The 2005 NOAA landcover database provides information on the dominant local vegetation which can be correlated to drag coefficients [16] [17].

Once this work is complete, higher flowrates will be modeled such that the river overflows its banks and modeled inundation of the floodplain will be compared to historical records of flooding.

Work is underway to develop the model to run in real time, providing daily updated seven day forecasts of river stage, tidal elevation, currents and inundation which will be made publicly accessible on the web. This information can then be used to better constrain and provide boundary forcing to the NOAA model currently in use to forecast for the West Pearl River.

V. Conclusion

A methodology has been developed allowing a mesh of a large region of the lower Pearl River in Mississippi and Louisiana to be developed at 4 m resolution from aerial

photographs. In the absence of measured bathymetry a "best guess" synthetic bathymetry has been fit to the channel by assuming a standard parabolic profile.

A subregion of this mesh has been validated against existing measurements and been shown to accurately predict water depth and currents at all measurement locations. The methodology to generate a synthetic bathymetry has been validated against the measured bathymetry in the East Pearl River and shown to be a realistic model in the main river channel but to be very inaccurate in coastal regions where sedimentation and scour can significantly affect channel morphology.

Plans are in place to further develop this mesh and extend it into the neighboring floodplains to allow modeling of the inundation of these plains tied to river flux, local runoff and storm events.

ACKNOWLEDGMENT

The authors would like to thank Alan Weidemann and Wesley Goode for their assistance in establishing and maintaining the moorings in the lower East Pearl River. We would further like to thank Dave Ramirez from the NOAA Lower Mississippi River Forecast Center for providing valuable information about the Western channel of the Pearl River. This work is supported under the NRL 6.2 Core Project "The Performance of a Persistent Riverine Surveillance Network". This paper is contribution number NRL/PP/7320–09-9337.

REFERENCES

[1] R. Patrick, *Rivers of the United States: Volume II Chemical and Physical Characteristics*. John Wiley and Sons, Inc., 1995.

[2] W. Thornbury, *Regional Geomorphology of the United States*. John Wiley and Sons, Inc., 1965.

[3] NASA, "Environmental resource document, inventory summary for John C. Stennis Space Center." 1992.

[4] C. Wax, "General climatology of Mississippi – Floods and droughts," in *National Water Summary 1988 - Hydrologic Events and Floods and Droughts, USGS Water Supply Paper 2375*. USGS, 1990.

[5] D. Turnipseed, G. Giese, J. Pearman, G. Farris, M. Krohn, and A. Sallenger Jr., "Hurricane Georges: Headwaters flooding, storm surge, beach erosion and habitat destruction on the Central Gulf Coast," USGS Water Resources Investigations Report 98-4231, Tech. Rep., 1998.

[6] H. Fritz, C. Blount, R. Sokoloski, J. Singleton, A. Fuggle, B. McAdoo, A. Moore, C. Grass, and B. Tate, "Hurricane Katrina storm surge distribution and field observations on the Mississippi Barrier Islands," *Estuarine, Coastal and Shelf Science*, vol. 74, pp. 12–20, 2007.

[7] H. Piatt, "The Jackson flood of 1979: A public policy disaster," *Journal of the American Planning Association*, vol. 48, no. 2, pp. 219–231, 1982.

[8] D. Gilvear, C. Davids, and A. Tyler, "The use of remotely sensed data to detect channel hydromorphology; River Tummel, Scotland," *River Research and Applications*, vol. 20, pp. 795–811, 2004.

[9] C. Legleiter, D. Roberts, W. Marcus, and M. Fonstad, "Passive optical remote sensing of river channel morphology and in-stream habitat: Physical basis and feasability," *Remote Sensing of the Environment*, vol. 93, pp. 493–510, 2004.

[10] S. Aarninkhof and J. Roelvink, "ARGUS-based monitoring of intertidal beach morphodynamics," in *Proceedings of the Coastal Sediments Conference*, 1999, pp. 2429–2444.

[11] H. Tanaka, "Monitoring of short-term morphology change at a river mouth," in *Proceedings of the Vietnam-Japan Estuary Workshop*, 2006.

[12] C. Blain, R. Linzell, and T. Massey, "MeshGUI: A mesh generation and editing tool for ADCIRC," Naval Research Laboratory, Tech. Rep. NRL/MR/7322–08–9083, 2008.

[13] A. Robert, *River Processes*. Hodder Arnold, 2003.

[14] R. Luettich, Jr. and J. Westerlink, "Combined discharge and radiation boundary condition in the ADCIRC hydrodynamic model: Theory and documentation," Department of the Army, Corps of Engineers, Tech. Rep., 2003.

[15] W. Emery and R. Thompson, *Data Analysis Methods in Physical Oceanography: Second and revised edition*. Elsevier, 2004.

[16] A. Lightbody and H. Nepf, "Prediction of velocity profiles and longitudinal dispersion in emergent salt marsh vegetation," *Limnology and Oceanography*, vol. 51, no. 1, pp. 218–228, 2006.

[17] C. Fischenich and S. Dudley, "Determining drag coefficients and area for vegetation," US Army Corps of Engineers, Tech. Rep. EMRRP SR-08, 2000.

McKay, P.; Blain, C.A.; , "Toward developing a hydrodynamic flow and inundation model of the lower Pearl River," *OCEANS 2009, MTS/IEEE Biloxi - Marine Technology for Our Future: Global and Local Challenges* , vol., no., pp.1-8, 26-29 Oct. 2009
Abstract: The lower Pearl River in Mississippi and Louisiana flows through extensive areas of intertidal marshes and flood-plains and is subject to frequent floods due to upstream flows, local runoff and tidal and storm forcing. In order to improve flow and flood prediction capabilities, a hydrodynamic flow and inundation model for the lower Pearl River is being developed using ADCIRC by the river modeling group at the Naval Research Laboratory at Stennis Space Center. Image analysis techniques are applied to high resolution aerial photography of the Pearl River to extract the channel boundaries and a synthetic bathymetry is generated by fitting an idealized cross-section across the channel. A mesh is generated for the entire lower Pearl River from Bogalusa, LA to the coast. A separate mesh is created for a subregion of the East Pearl River and this model is validated against observations.
URL: http://ieeexplore.ieee.org/stamp/stamp.jsp?tp=&arnumber=5422419&isnumber=5422059